Surface & Coatings Technology 374 (2019) 21–31

Contents lists available at ScienceDirect

Surface & Coatings Technology

journal homepage: www.elsevier.com/locate/surfcoat

Heat-treatment and mechanical properties of cold-sprayed high strength Al alloys from satellited feedstocks

Kamaal S. Al-Hamdani[a,c], James W. Murray[a], Tanvir Hussain[b], Adam T. Clare[a,d,*]

[a] Advanced Component Engineering Laboratory (ACEL), University of Nottingham, Nottingham NG7 2RD, UK
[b] Advanced Materials Research Group, University of Nottingham, Nottingham NG7 2RD, UK
[c] University of Thi-Qar, College of Engineering, 64001 Nasiriya, Iraq
[d] Department of Mechanical, Materials and Manufacturing Engineering, Faculty of Science and Engineering, University of Nottingham China, 199 Taikang East Road, University Park, Ningbo 315100, China

ARTICLE INFO

Keywords:
Satelliting
Metal-ceramic
Cold spray
Porosity
Annealing
Coatings
Titanium carbide
Aluminium 6061

ABSTRACT

In prior work, the authors demonstrated a method for the creation of composite coatings containing TiC particles in a pure Al matrix by cold spray via a satelliting technique. Here, the authors investigate the effects of using the 'Satelliting' technique on the deposition and characteristics of A6061-TiC coatings fabricated by cold-spray. The results showed clear improvements in the deposition efficiency and porosity of the satellited powder obtained by using the satellited feedstock. Annealing heat-treatment was then applied for further enhancement of the coating's density and wear properties. The heat-treated coating exhibited a ~70% reduction in interlamellar porosity. Dry sliding wear testing using a steel counter body at 5 N showed that using a satellited feedstock with TiC yielded a 55% and 20% reduction in coating specific wear rate in comparison to coatings made using pure 6061 and blended 6061-TiC, respectively. This was further reduced by ~70% and 40% in comparison to the 6061 and blended 6061-TiC coating after heat-treatment with good repeatability.

1. Introduction

Ceramic-reinforced metal matrix composites are desirable given their combination of metallic properties; such as high ductility, toughness, and thermal conductivity alongside ceramic characteristics of high hardness, high strength and Young's modulus [1]. Aluminium-matrix composites (AMCs) are an example of such a material type, which can possess both corrosion resistance and hard-wearing properties [2–4]. Additionally, aluminium is able to alloy with a large number of elements, including magnesium, silicon, copper, manganese and zinc, hence providing specific, tailorable properties to the resultant composite [5].

Aluminium 6061 is widely used in many automobile, aerospace and mineral processing components because it boasts low density and high electrical/thermal conductivity [6]. These alloys have exhibited a high corrosion resistance and considerable formability among other aluminium alloys as well as offering a greater strength- to weight ratio. In addition, 6061 composites that are reinforced with ceramic particles have been effectively used because of properties such as high strength at high operation temperature, good fatigue and stiffness properties [7]. Limited studies have been reported on depositing 6061 alloy powder or its composites. Rokni et al. [8] reported that, owing to its relatively high strength, 6061 shows a lack of deformation within cold sprayed deposits even when using high temperature processing (400 °C), that leads to the production of a high porosity coating. In another study, cold-sprayed 6061 alloy coating showed a higher strength and lower elongation than the wrought and annealed alloys due to strain hardening associated with the cold spray process [9]. Consequently, it is a challenge to deposit dense 6061 coatings using cold spray with both gas and substrate at room temperature.

Cold spray (CS) is a solid-state deposition process that accelerates powder particles to a high velocity (usually 500–1200 m/s) [10], resulting in collision with a substrate or with already deposited material. It is an example of a manufacturing process capable of producing coatings of typically soft materials with a wide range of thicknesses (25 μm to several centimetres). Cold-spraying is advantageous over competing technologies in many cases, including high velocity oxy-fuel and plasma spraying, as the lack of melting means the properties of the starting material can be maintained. Compressive residual stresses are also typical in cold-sprayed coatings which may be advantageous for mechanical properties [11]. In addition to metals, deposition of various CS coatings has proven to be possible including composites, ceramics

* Corresponding author at: Advanced Component Engineering Laboratory (ACEL), University of Nottingham, Nottingham NG7 2RD, UK.
E-mail address: adam.clare@nottingham.ac.uk (A.T. Clare).

https://doi.org/10.1016/j.surfcoat.2019.05.043
Received 2 January 2019; Received in revised form 5 March 2019; Accepted 15 May 2019
Available online 16 May 2019
0257-8972/

Table 1
Nominal chemical composition of Al 6061 powder and Al 6082-T6 substrate [53].

Element (%)	Si	Mg	Mn	Fe	Cr	Zn	Ti	Cu	Others	Al
Al 6061	0.4–0.8	0.8–1.2	0.0–0.15	0.0–0.7	0.04–0.35	0.0–0.25	0.0–0.15	0.0–0.1	0.0–0.15	Balance
Al 6082	0.7–1.3	0.6–1.2	0.4–1.0	0.0–0.5	0.0–0.25	0.0–0.2	0.0–0.1	0.0–0.1	0.0–0.15	

and polymers [12–14]. Bonding and coating build-up takes place by plastic deformation of the incident particles, as well as the substrate surface to some extent, leading to the formation of coatings without the need for additional heating [8]. This means that material structure and composition are maintained relative to the feedstock [10]. As a result of the plastic deformation mechanism of CS, embedment of ceramic materials is problematic since these do not plastically deform upon impact, and hence rebound [4]. Furthermore, it is reported that a shock wave forms ahead of the substrate surface with a bow shape as a result of the impingement of the supersonic gas jet [15]. This shock wave makes fine particles ($< 5\,\mu m$) lose a significant amount of velocity before impacting the substrate surface. This reduction in particle impact velocity can reduce the possibility of producing a sufficient deformation for the fine metallic particles as well as increase the likelihood of rebound of hard particles.

Satelliting was recently used as a method for preparing composite feedstocks [16], depending on using a liquid binder to attach fine (satellite) particles onto relatively large metallic (parent) particles. Satelliting is a technique which could fall under the umbrella definition of wet granulation [17]. It is specifically well suited to the controlled adherence of small reinforcement particles to a larger 'planet' particle. Readers can refer to the related patent [16] should they require further information. This technique was successfully used to prepare composite feedstocks of various deposition techniques such as cold spray [18] and direct metal deposition [19,20]. In the authors' prior work [18], to overcome the problem of deposition of ceramic materials, satelliting of small ceramic particles (TiC) to parent aluminium particles via use of a binder was demonstrated as an effective method of significantly increasing the level of ceramic attachment in the CS coatings. Although the principle of formation of a TiC reinforced AMC composite was demonstrated evaluation of properties was not undertaken.

Annealing has been shown to reduce the porosity of cold-sprayed Al coatings, enhancing inter-splat bonding [21,22]. This has also been shown to improve toughness and tensile properties of the cold worked aluminium alloys [23]. Chavan et al. [24] pointed out that increasing the heat treatment temperature led to a reduction in the cold work, structure and inter-splat porosities of the cold sprayed coatings. Pitchuka et al. [25] stated that a dense structure with a reduction of 60% in porosity can be achieved due to solid state diffusion occurring during the heat treatment of the Al cold sprayed coating. Huang et al. [26] have heat-treated a cold-sprayed coating of commercially pure aluminium where diffusion, recystallisation as well as some grain growth explained the notable reduction in porosity over a temperature range of 300–400 °C. The presence of hard particles (e.g. ceramic) in the metallic feedstocks improves the deposition of the metallic particles in cold spraying, it also contributes in improvement in mechanical properties, densification of the coating structure and enhancing of process stability [27]. Two suggested mechanisms explained the role of ceramic particles in enhancing the deposition of aluminium in cold spraying [28]. Firstly, the creation of micro-asperities improves the mechanical bond between the Al particles. Secondly, breaking up of the oxide layer prepares oxide-clean surfaces that facilitate the bonding process [29]. It is observed that the use of fine ceramics has an important impact on the deposited coating as the fine size lead to a reduction in the mean free path and thus improvement in the mechanical properties [30]. Additionally, it is found that fine ceramic particles more effectively contribute to the cohesion of cold sprayed coatings, while the loose coarse ceramic particles are more detrimental to coating cohesion [29].

In the present study, cold spraying is used to create composite coatings of 6061 aluminium alloy reinforced with TiC particles on an A6082 aluminium substrate using optimised spray conditions previously determined. A6061 coatings were also cold sprayed using identical process conditions for comparison. The satelliting technique was used to prepare the composite feedstock to eliminate the rebounding of the fine ceramic fraction in the CS process. Annealing heat treatment was applied to the composite CS coatings to reduce porosity and improve cohesive properties of the coating structure. Additionally, a detailed hardness study is performed to evaluate hardness prior to and after heat treatment so the effect of heat treatment on matrix as well as overall composite properties can be understood. Dry-sliding wear testing is performed to evaluate the contribution of the reinforcement material to as well as the effect of heat treatment on practical mechanical properties.

2. Experimental details

2.1. Materials

6061 aluminium alloy (simply 6061) was used as the parent powder and TiC as a reinforcement material in the satelliting process to prepare a composite satellited feedstock (6061-TiC) for processing by cold spray. The Al powder has an irregular shape with 20–53 μm size range ($D_{(50)} = 36.5\,\mu m$); provided by LPW Technology, UK. This powder was also used as a 6061 feedstock for comparison (without satelliting). The nominal chemical composition of this powder is shown in Table 1. The angular TiC powder has a particle size $< 5\,\mu m$ with a mean particle size of 3 μm, supplied by GoodFellow, UK. The binder was lab prepared by dissolving a 2.7% of polyvinyl alcohol (PVA) in 97.3% water by volume (4.05 g PVA in 100 g water). For comparison purposes, simple blended 6061-TiC feedstock was also prepared by mixing the same powders with the same weight fractions but without the use of liquid binder. Grit blasted 6082 aluminium plates ground using 240-mesh grit were used as substrates for CS with dimensions of 25 × 50 × 6 mm. This material was used as it is a commonly used aluminium alloy with similar properties to the powder. The nominal chemical composition is shown in Table 1 below.

2.2. Feedstock preparation

The batch of satellited feedstock used for cold spray was made via multiple small batches of 25 g which were consecutively satellited using the incremental addition of binder and gyroscopic mixing until reaching the desired quantity. The final feedstock consisted of 80 wt% 6061 and 20 wt% TiC with a negligible amount of remaining binder (~0.0007 wt%).

2.3. Cold spray

Cold-spraying was performed to create individual tracks of 6061, blended 6061-TiC and satellited 6061-TiC on Al substrates. The CS system used for this work is a custom built system described in detail elsewhere [31]. The system consists of a helium and nitrogen gas pressure system, a commercial powder feeder (Praxair 1264HP, Indianapolis, IN, USA) with a 12-slot feeding wheel, which has a changeable rotating speed. The gun is a steel de-Laval nozzle with a throat diameter of 1.35 mm, an area expansion ratio of ~8.8 and a

Table 2
Cold spray deposition parameters for single tracks.

Transverse speed (mm/s)	Stand-off distance (mm)	Stagnation pressure of main gas (bar)	Stagnation pressure of carrier gas (bar)
60	20	28	29

divergent section of 150 mm length. The nozzle exit diameter is 4 mm. The standoff distance between the nozzle and the substrate surface was fixed at 20 mm. The transverse speed of the spraying table in two-dimensions is computer-controlled, with three systematic parameters considered as shown in Table 1. Helium at 2.8 MPa was used in the spraying system for the primary accelerating gas at room temperature, while nitrogen was used as the powder carrier gas at 2.9 MPa. Helium working gas was used due to its better performance at lower pressures. Substrates were clamped onto the spraying table, which controls the relative motion between the substrate surfaces and the nozzle (Table 2).

2.4. Heat treatment

6061 and 6061-TiC coating samples were subject to an annealing heat treatment at 345 °C for a duration of 2 h. These parameters are well understood to relieve the strain hardening effects of cold worked 6061 components [23,32]. The annealing process has been reported as an effective method for reducing the porosity of cold-sprayed Al coatings [25]. It has also been reported that the metallurgical bond in the cold-sprayed coatings has been enhanced throughout the annealing process due to the solid state diffusion that occurs [22]. A tubular furnace (Lenton Thermal Designs LTD, UK) with an accuracy of ± 5 °C and heating rate of 10 °C/min was used in these experiments. The samples were furnace cooled to room temperature. Argon was used as a shielding gas (1 l/min) during the heat treatment process in order to protect the sample surface from oxidation.

2.5. Powder and coating characterisation

Scanning electron microscopy (SEM) with an FEI Quanta 600 was used to confirm successful satelliting of the powder, as shown in Fig. 1. Significant coating of the large aluminium particles by TiC can be seen, however it should be noted that some particles are not successfully coated given the stochastic nature of the mixing process, and in particular difficulty in achieving a uniform spread of binder.

Fig. 2 shows the particle size distribution of the 6061 and 6061-TiC feedstocks. This is a useful way of illustrating the extent of satelliting. The results show that the majority of TiC particles were satellited as only 25% of the TiC particles are shown in the data in Fig. 2(b). This was calculated by converting the volume fraction of the free TiC that presents in the particle size distribution data into weight fraction by considering the density of TiC. This implies that 75% of the original TiC by weight was satellited to the Al particles.

Cross-sectional imaging was performed on samples after polished using SiC grinding wheels final polishing stages using 6 and then 1 μm diamond paste.

Image-J software (USA) was used to analyse the thickness and porosity of the deposited coatings using three SEM across the length of the coatings using images of 250 × 350 μm to provide averages. All error bars represent the standard error values of the mean of the relevant measurements. The deposition efficiencies (Fig. 4) were also measured as the ratio of the coating deposition mass to the mass of sprayed powder during the processing time [33].

A Buehler Microhardness machine (USA) was used for microhardness testing on coating cross-sections, using loads of 10 gf and 50 gf and a dwell time of 15 s. At both loads the average of 10 Vickers microhardness measurements was used to provide mean hardness values. The distance between every two consecutive indents was kept 5 times more than the indent size to avoid the influence of nearby indents on the next indent. To examine phase composition of the sprayed coatings, a Siemens D500 X-ray diffraction instrument was used, with a wavelength of 0.15406 nm (Cu k-alpha), a 2θ range of (30°–90°) and step size and step time of 0.05° and 2 s, respectively. Ball-on-flat reciprocating dry-sliding wear tests were performed using AISI steel ball (grade 440c) with a hardness of 250 Hv, and 6 mm diameter as a counter body at 5 N normal load. A CETR Universal Micro-Tribometer 3 (USA), was used for all wear tests, using a linear displacement amplitude of 5 mm and 1 Hz frequency for a duration of 10 min. A sample of 25 × 50 mm of each coating type was prepared for wear tests, using an overlap cold-spray strategy. The coated area was 35 × 25 mm with an average thickness of ~300 μm. All coating surfaces were polished to a mirror finish using standard grinding and polishing steps, finishing with a 1 μm diamond polish prior to testing. Three tests were performed on each sample to confirm result reliability. An Alicona Infinite Focus focus variation microscope was used to measure wear track volume. The specific wear rate (SWR) was calculated using the following formula:

$$\mathrm{SWR} = \frac{wear\ volume\ (mm^3)}{load\ (N) * distance\ (m)}\ (mm^3/\mathrm{Nm}) \quad (1)$$

where the wear volume is the track area (average) multiplied by the track length (5 mm), load is 5 N and the total worn distance during the test is 6 m. SEM was used to analyse the worn surfaces of wear tracks.

3. Results and discussion

3.1. Coating characterisation: Al 6061 vs Al6061-TiC

Typical cross-sectional BSE images of the 6061 and 6061-TiC coatings are shown in Fig. 3. The structure of the 6061 coating is presented in Fig. 3-a. The 6061 particles were deformed on impact as is typical to cold-spray. Fig. 3-b shows the cross-section morphology of the blended 6061-TiC coating, wherein the irregular bright particles are TiC particles on the grey metallic matrix. Both 6061 and blended 6061-TiC coatings contain significant interlamellar porosity and open boundaries in their structure, distributed over the coating. In addition, the interface of the coating/substrate can be clearly seen. Fig. 3-c shows the cross-section morphology of the satellited 6061-TiC coating. A higher level of local deformation and larger TiC area fraction with an improved distribution can be clearly noticed in the satellited coating. The enhanced distribution of the ceramic is consistent with the boundaries of aluminium particles. It can be seen that porosity was greatly reduced in the satellited coating, and the coating/substrate interface became much less visible in the 6061-TiC coating indicating an improved adhesion between the coating and the substrate.

As cold spray greatly depends on the deformation of the sprayed materials, an absence of particle deformation can lead to porosity. Significant porosity can be seen in the 6061 coating, which can be explained by a lack of local deformation. Additionally, the appearance of the interface line indicates poor bonding in several substrate-coating interface regions. This is correlated with the low ductility of 6061 that causes limited local deformation of the deposits. Low particle deformation produced poor particle-particle interfacial bonding and created a highly porous structure as shown in Fig. 3-a. For the blended coating, the presence of the TiC particles has affected the level of porosity. This can be explained by the effect of ceramic particles on increasing the local deformation at the impact surfaces, as the TiC particles appear clearly inserted in the matrix splats. This made the blended coating presents lower porosity than 6061 coating. Fig. 3-c shows the low porosity, well-bonded coating characteristic of the satellited feedstock. Similar results were also observed showing the clear contribution of ceramic particles in enhancing the bonding between the deposited Al splats as well as between the coating and substrate [34,35].

Fig. 4 shows thickness and deposition efficiency (DE) data for the as-

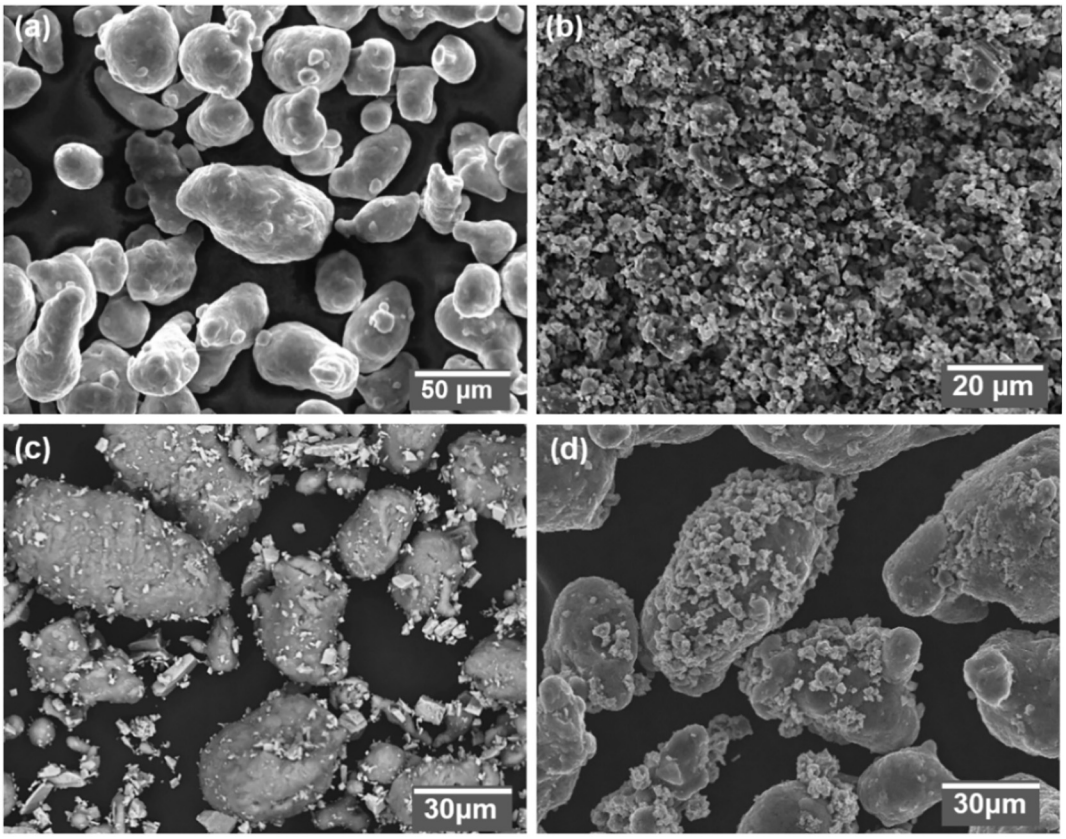

Fig. 1. SEM SE images showing the morphology of (a) virgin 6061 powder (b), virgin TiC powder, (c) blended feedstock (6061-TiC) and (d) satellited feedstock (6061-TiC).

sprayed 6061 and 6061-TiC blended and satellited coatings. It can be seen that the blended 6061-TiC coating had the lowest thickness (240 µm) and lowest DE (18%) among the coatings, while the 6061 presents an average thickness of 268 µm. It is believed that the free TiC particles have potential to rebound after impact, especially when hitting a low-ductility surface i.e. 6061. This means a significant portion of the reinforcement particles are lost, leading to a reduction in surface activation by producing micro-asperities on the impact surfaces and deposit interlocking. This also caused the 6061 and blended coatings to have a similar thickness measures particularly when error bars are taken in consideration. It is conceivable that impingement of the hard particle results in a peening/densification effect in the deposited coating, reducing interlamellar porosity, and this effect is still present despite significant rebound of the particles. This would be similar to the shot-peening (SP) particles that are used for tamping CS coating [36], where steel particles mixed and sprayed with Al powder to compact the deposited Al particles before rebounding.

The satellited 6061-TiC coating yielded the larger thickness (360 µm) with an increase of 34% and 50% compared to the 6061 and blended 6061-TiC coatings, respectively. In addition, as represented by the error bars, the satellited 6061-TiC coating was more uniform in thickness than blended coating, reaching a minimum of 340 µm and maximum of 380 µm. The DE of the satellited 6061-TiC coating is clearly higher than the 6061 and blended 6061-TiC coatings (Fig. 4-b). This also confirms the improvement in the material deposition regime of the satellited feedstock when compared with 6061 and blended 6061-TiC coatings because of the presence and behaviour of the satellited hard particles. A similar trend was observed in previous studies; for instance, it was found that the addition of ceramic particles in simple mixing enhances the deposition efficiency (DE) of aluminium composite coatings [21]. This was due to reducing the critical velocity and creation of asperities in the coating during spraying that facilitated the bonding of incoming Al particles.

In the satellited feedstock, the attachment of TiC particles on an Al particle surface will increase the Al particle mass by 25% compared to a non-satellited Al particle with the same size, assuming all TiC particles are attached to the Al particles. This increase in particle mass leads to a reduction in the in-flight velocity of the satellited particle due to the increase in both density and particle diameter according to the particle velocity Eq. (2), [37].

$$v_p \approx \left[\frac{c_2}{\sqrt{R\,T_o}} + \sqrt{\frac{\rho_p d_p}{C_d L_d p_0}} \right]^{-1} \tag{2}$$

where;

v_p: in-flight particle velocity	C_2: fitting parameter = 0.45 for helium
R: gas constant = 2077 (J/kg-K°)	T_o: gas stagnation temperature = 290 K°
ρ_p: particle density,	D_p: particle diameter (45 µm)
C_d: drag coefficient = 0.47	L_d: length of the diverging part of the nozzle = 150 mm.
P_o: gas stagnation pressure 2.-8 bar	

For a 45 µm diameter Al particle, after satelliting, the density of the satellited particle increases from 2.7 (Al density) to 2.968 g/cm^3, this was obtained by determining the whole weight and volume of the satellited components. While the particle diameter increases from 45 to 46.97 µm obtained by adding the volume of the satellited TiC as a thin layer evenly distributed on the Al particle surface. Therefore, the particle velocity has decreased by 4% (from 740 to 711 m/s) due to the increase in both density and particle diameter values in the equation. The momentum of the satellited particle can be expressed by the new mass and velocity values of the satellited particle, as follows:

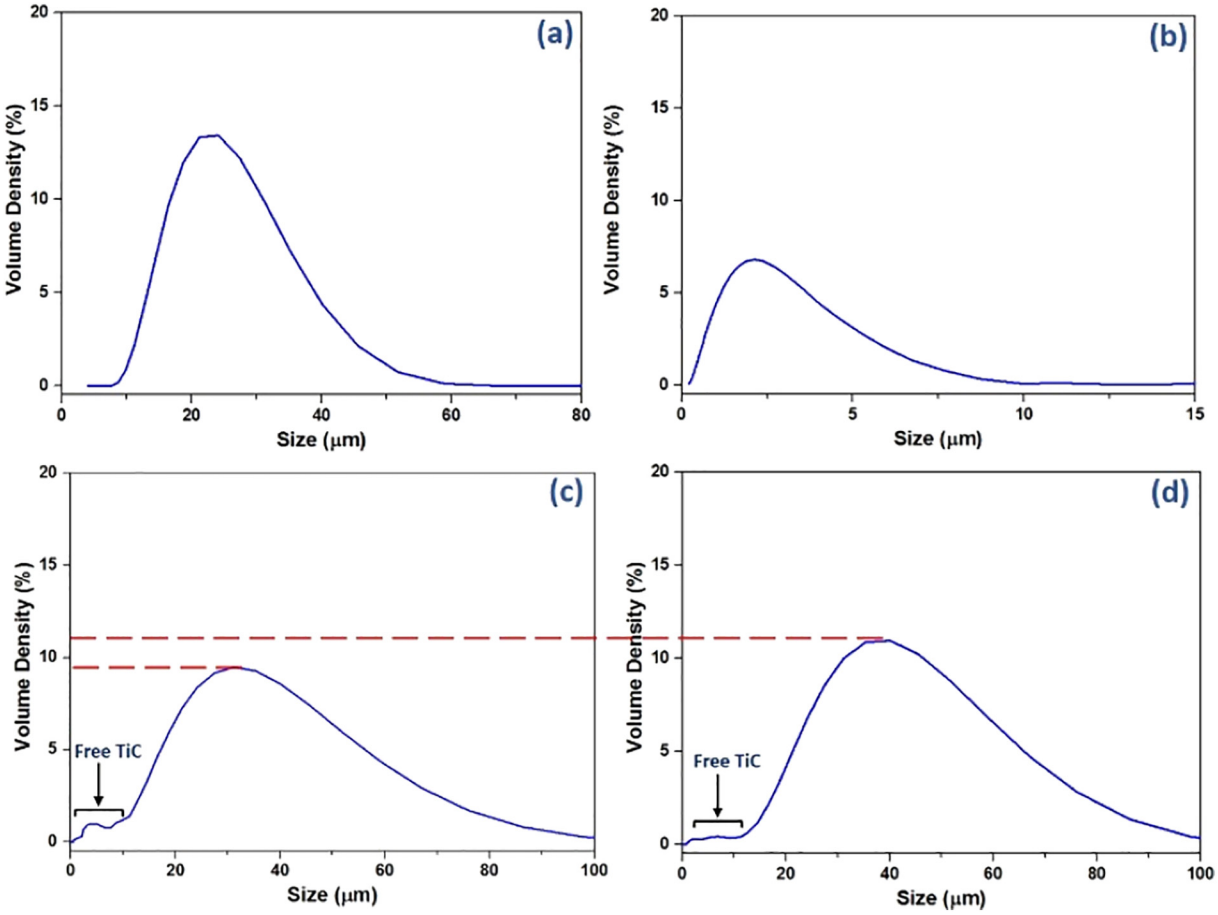

Fig. 2. The particle size distribution of (a) 6061 powder (b), TiC powder, (c) blended feedstock (6061-TiC) and (d) satellited feedstock (6061-TiC).

$$M = v \times m \tag{3}$$

For an Al particle (not-satellited):

$$M_{Al} = v_{Al} \times m_{Al}$$

After satelliting;

$$v_s = 0.96\, v_{Al};\ m_s = 1.25 \times m_{Al}$$

$$M_s = 0.96\, v_{Al} \times 1.25 \times m_{Al} = 1.2\,(v_{Al} \times m_{Al})$$

$$M_s = 1.2\, M_{Al} \tag{4}$$

According to Eq. (4), the satellited particles gained 20% higher momentum than the non-satellited Al particles with a same particle size. This may explain the lower level of porosity due to the greater peening action of the satellited particles. In addition, it is known that the deposition of cold-sprayed materials greatly depends up on the mechanical/metallurgical bonding created by local plastic deformation [38]. Thus, the satellited particle that has a layer of hard particles with higher momentum has the ability to produce a higher level of plastic deformation in the coating, increasing material deposition. This could also explain the higher DE and thickness of the satellited 6061-TiC among the coatings.

Fernandez and Jodoin [28], have proven that the micro-asperities made by the impact of angular ceramic particles have a significant contribution in increasing the DE of Al particles. They showed that these asperities were produced by cutting of the metal and rebounding of the sharp-edged ceramic particles. Namely that it is needed to rebound more ceramic particles to create more asperities for increasing the DE of the matrix metal. In case of satellited feedstock, the satellite particles (i.e. TiC) are entrapped between the existing and incoming 6061 particles, causing TiC to be retained in the coating. This will simultaneously increase the deposition of both matrix and ceramic particles because creation of asperities increases, as the ceramic deforms both incoming and already deposited particles, and rebounding of TiC decreases. As discussed in the authors' previous work, this mechanism of embedment of the TiC is based on TiC remaining attached to the parent particles upon impact [18]. In particular, it has been observed that the trapping of TiC beneath the impacting particle is key to retaining significant TiC content. Consequently, this improvement in material deposition can explain both the larger thickness and higher DE measurements of the 6061-TiC coating compared with the 6061.

Porosity levels in the deposited coatings are shown in Fig. 5. The 6061 coating presents a high level of porosity (4.94%) compared to (2.06%) of the blended 6061-TiC coating, and (0.66%) of the satellited 6061-TiC coating. The most likely reason for the interlamellar porosity in CS coatings is the lack of deformation at particle sides [11]. The presence of TiC particles in the blended feedstock decreased the porosity by about 60% compared to the 6061 coating. This is explained by the effect of hard particles on increasing the local deformation and enhancing bonding of splat surfaces. Similar results were observed by Koivuluoto and Vuoristo [39], in which it was stated that the activation, cleaning (removing impurities and contamination from the impact surfaces) and hammering actions of the ceramic particles (Al_2O_3) have significantly reduced the porosity of the CS Ni-20Cr-Al_2O_3 coating. However, the rebound of an important portion of TiC during the cold spray process decreased the effectiveness of TiC in reducing the porosity more, see Fig. 6. It is shown that the satellited feedstock presents a clear superiority in depositing hard particles (TiC) in the cold sprayed Al coating. The deposition efficiencies of the ceramic particles of the blended and satellited feedstock were 29% and 48%, respectively. These were calculated by comparing the volume fraction of the TiC

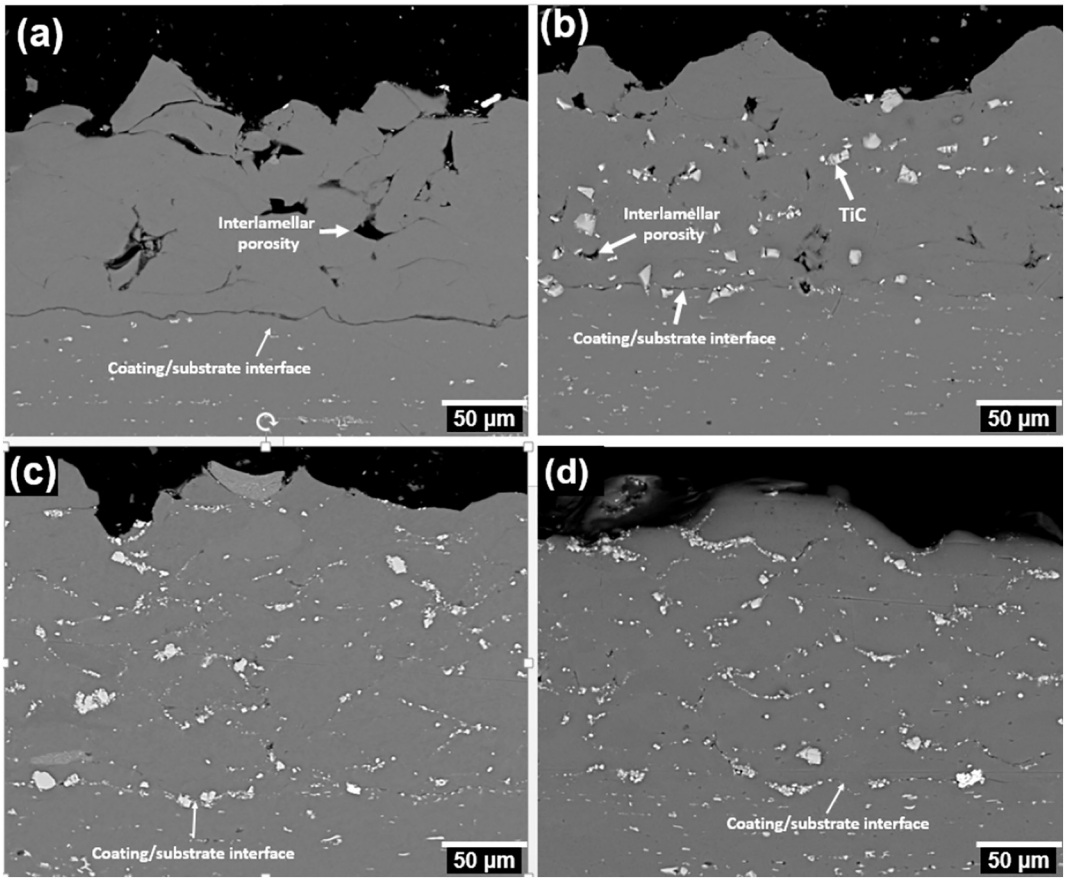

Fig. 3. Cross-sectional BSE images showing the different structures of the cold sprayed coatings; (a) 6061 coating, (b) blended 6061-TiC, (c) as-sprayed 6061-TiC satellited coating and (d) heat-treated 6061-TiC satellited coating.

between the coating sections and starting materials through converting weight fractions into volume fractions depending on the material densities.

The satellited 6061-TiC coating shows a significant reduction in the interlamellar porosity, it is lower than the 6061 coating and blended 6061-TiC coating by 87 and 68%, respectively. The effect of the TiC particles on coating porosity is similar to their actions in the case of the blended coating. Moreover, the larger TiC fraction can increase the influence of TiC particles in the satellited coating. In addition, it was found that the hard particles with high momentum allow a higher level of deformation and also increase the peening action in the cold-sprayed layers [40]. Thus, the satellited particles that have a higher momentum (Eq. (4)) and hard–grainy surface, have the potential to carry out the compaction process in an improved manner. This can explain the eliminated porosity and dense structure of the satellited 6061-TiC coating in comparison to 6061 and blended 6061-TiC coatings (Fig. 3).

3.2. Effect of heat treatment on the satellited coatings

In order to obtain further improvement in structure density and coating cohesion, the satellited 6061-TiC coating was heat treated at 345 °C for a duration of 2 h. This temperature is above the re-crystallization temperature of Al, which is 325 °C [41]. Fig. 3-d shows a BSE image of cross-sectional area of the heat-treated satellited coating.

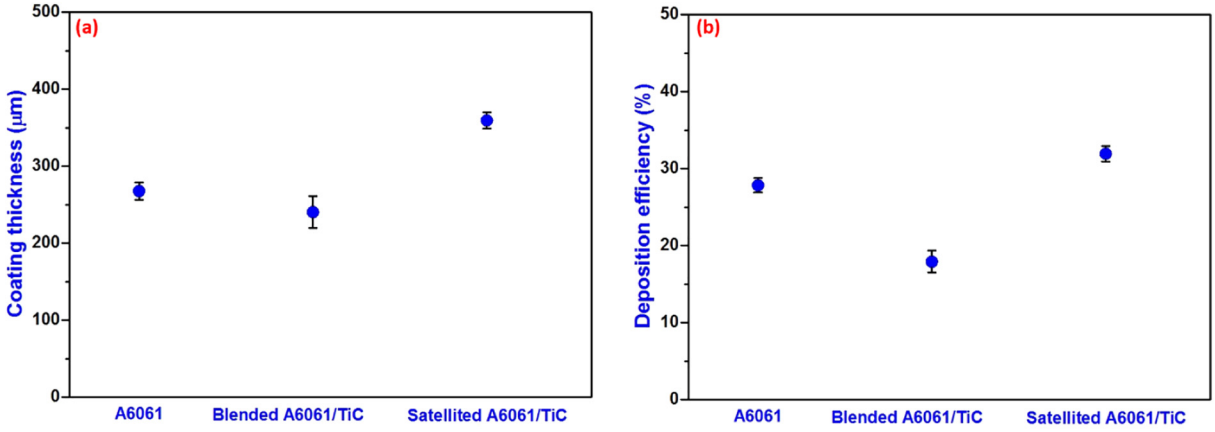

Fig. 4. (a) The average thickness and (b) the deposition efficiency of the deposited coatings.

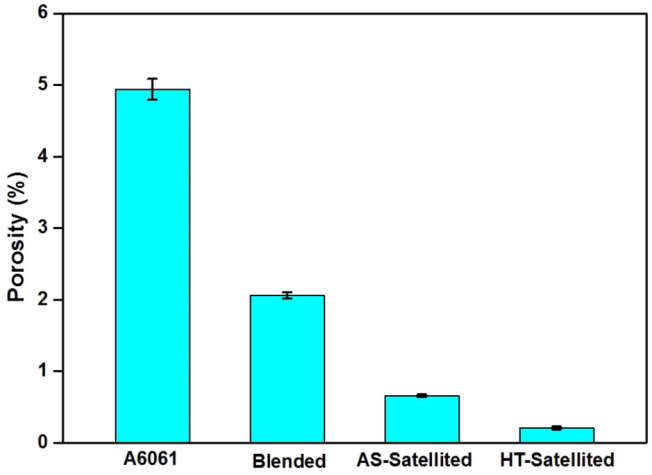

Fig. 5. The percentage porosity by area of the deposited coatings, showing the effect of addition of TiC and heat-treatment on coating porosity.

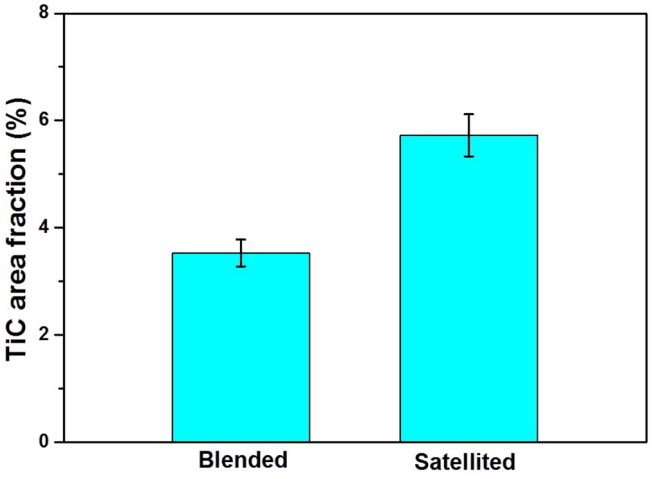

Fig. 6. TiC area fraction in the coating section showing the contribution of satelliting in increasing the embedded ceramic.

The annealing process caused ta reduction in interlamellar porosity and healing of most inter-splat and coating/substrate interface lines. Although the as-sprayed satelliting coating retained only 0.66% porosity, this was decreased after heat treatment to 0.21%. This level of porosity is 50% of the 6061 based CS coating achieved by Wei et al. in their 'fully dense coating' [36]. Consequently, a superior coating in terms of porosity level and structural cohesion particularly after heat treatment can be achieved by using the satellited feedstock. In addition, the range of data for porosity for the heat-treated coating is notably reduced.

Similar observations were made in a previous study, in which the interlamellar porosity of cold-sprayed Al coatings significantly decreased after annealing at 300 °C [25] owing to solid state diffusion in the inter-splat boundary regions. The self diffusion coefficient of Al at 345 °C is 5.23×10^{-16} (cm^2/s) as reported by Messer et al. [42]. Accordingly, the expected diffusion distance of the aluminium atoms after 2 h will be 1.94 µm. Thus, it is supposed that an interlamellar pore of 2 µm size can be 'sealed' by the diffusion of Al after 2 h of annealing at 345 °C. This can explain the consequence of the annealing process regarding the structure densification of CS coatings. The contribution of the heat treatment processes in improving CS coating structure was reported in previous studies [24–26], however without demonstrating the potential of diffused materials to reduce the porosity. Li et al. [22] reported that the heat treatment process can be used to improve the inter-splat metallurgical bond between the CS splats due to diffusion at

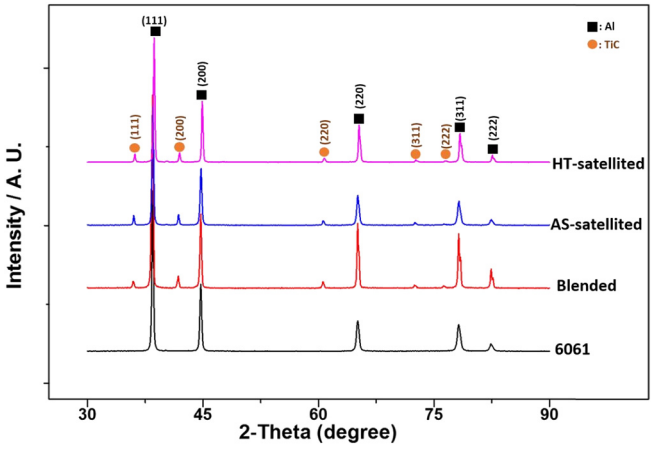

Fig. 7. X-ray diffraction patterns of the deposited coatings.

grain boundaries. These observations can confirm the impact of annealing on enhancing the CS coating porosity by diffusion at the splat boundaries.

XRD analysis was performed on the three coating types. XRD patterns of the as-sprayed 6061, labelled 6061-AS and heat treated satellited 6061-TiC, labelled as 6061/TiC-HT coating samples are shown in Fig. 7. Similar patterns were obtained for the blended and both AS and HT satellited 6061-TiC coatings. There is no indication that the heat treatment resulted in formation of intermetallic components or oxides of the alloy components in the coating. The annealing temperature was lower than that required for the formation of intermetallic components between Al and TiC [43,44]. Similarly, it is also clear from Fig. 7 that there is no noticeable difference in the two patterns of the as-sprayed and heat-treated satellited 6061-TiC coatings, confirming that there were no intermetallic structures formed due to the annealing process in these conditions.

A series of 50 gf microhardness measurements were used to evaluate the practical hardness of the coating, by creating indents which incorporate both matrix and ceramic material. Fig. 8 shows the measured microhardness values of the deposited coatings. The as-sprayed satellited 6061-TiC coating presents the highest mean microhardness value among the coatings at 91 HV0.05 (± 1.5). The mean hardness of the heat-treated 6061-TiC was 83 HV0.05 (± 0.7), while the as sprayed 6061 coating yielded 70 HV0.05 (± 0.8). The blended 6061-TiC coating presented a hardness similar to the 6061 coating, 67 HV0.05 (± 1.8), with a higher range among the coatings confirmed by the larger error bars. This can indicate a non-uniform structure density and

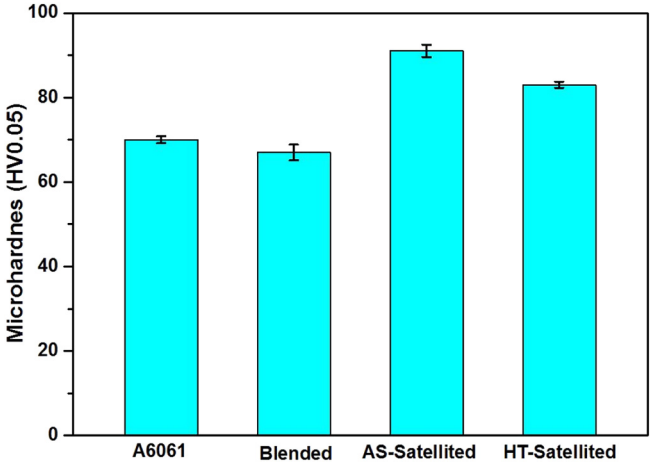

Fig. 8. Microhardness measurements at the centreline of the deposited coatings.

TiC distribution of the blended coating. It is known that the high strain hardening of the cold work associated with cold spray leads to the creation of high residual stresses in the CS coatings [45]. The higher hardness of the AS-satellited 6061-TiC coating is related to two combined factors; the higher level of deformation due to the satellited feedstock behaviour (higher momentum), and the presence of a larger amount of the reinforcement in the coating structure. The TiC area fraction also increased by > 60% in the coating section compared to the blended coating, Fig. 6. It is known that the reinforcements have a marked effect on the mechanical and microstructural properties of the coatings, and they increase with increasing the amount of the entrapped ceramic particles [27].

After heat treatment, internal residual stresses are expected to be relieved, hence also contributing to a lower measured microhardness in the heat-treated coatings. These results are in agreement with another prior study [46], in which the hardness of the aluminium alloy (5083) cold-sprayed coating decreased after annealing heat treatment. This was explained by grain recovery, i.e. a reduction in dislocation density, which would also explain the reduced hardness in the case of cold-sprayed coatings which have been subject to work hardening. However, the HT-satellited 6061-TiC coating still has a hardness value higher than the 6061 coating. This is explained by the contribution of the ceramic particles to the resistance to indentation at this load level. The HT-satellited 6061-TiC coatings showed a minor reduction in mean hardness, however they are similar when considering the error range. To determine in more detail the contribution of factors to the hardness measurements, Fig. 9 shows microhardness indents at 10 and 50 gf loads that were made on the deposited coatings, noting the smaller scale of (e, f, g and h).

The microhardness of the AS and HT coatings was also measured using a smaller load (10 g) targeting TiC-free areas, as shown in Fig. 9(e–h), in order to determine the contribution of TiC addition and heat treatment on matrix properties. The Vickers microhardness measurements of the Al matrix (HV0.01) in the as-sprayed and heat-treated satellited 6061-TiC coatings were 79 and 65 HV0.01, respectively, compared with 61 HV0.01 of the 6061 coating. The blended 6061-TiC presented a microhardness of 64 HV0.01.

The increase of the matrix hardness in the AS satellited 6061-TiC coating can be explained by the increased work hardening in the composite cold-spray coatings, this is likely result of the high level of work hardening caused by the satellited particles during CS process. While the annealed matrix showed lower hardness values than the as-sprayed coating owing to the softening action of the annealing process, however it still had a hardness higher than the 6061 coating due to the TiC reinforcing effect. It is therefore clear that the addition of TiC provides the majority of the hardness increase as measured by the 50 gf indents for the results in Fig. 8. These results are consistent with results of a recent study [40], it was found that the higher level of work hardening, caused by the high momentum of hard particles, led to a significant improvement in the matrix hardness and wear resistance of the cold sprayed coatings. In fact, the slightly lower mean hardness value of the heat-treated coating implies that the annealing and softening effect of the heat-treatment plays a more significant role.

When a large load was used (50 gf), some cracks can be seen adjacent to the indents on the AS-6061 and AS-composite coatings, but not at the indent tip. It is observed that cracks do not necessarily start from the indent corners in the sprayed coatings [47], due to the inhomogeneous structure. The inter-splat cracks take the direction parallel to the substrate-coating interface which is consistent with the direction of elongation of splats [48]. On the other hand, there is no cracking or inter-splat cracking observed at the indents made in the heat-treated coatings. This may indicate an improvement in the fracture toughness of the HT coating, owing to matrix softening and enhancement of the interfacial bonding as a result of the annealing process.

3.3. Wear behaviour of the deposited coatings

Fig. 10 shows the specific wear rate (SWR) of the deposited coatings; 6061, blended 6061-TiC, AS-satellited 6061-TiC and HT-satellited 6061-TiC under dry sliding wear conditions. It can be seen that the SWR of the satellited 6061-TiC coatings (AS and HT) was lower than the other coatings. The SWR of the AS-satellited 6061-TiC was 55% and 20% lower than that of 6061 and blended 6061-TiC, respectively. This can be explained by the contribution of the reinforcing TiC particles in increasing the hardness, as well as reducing porosity, hence resulting in increased wear resistance.

Interestingly, the heat-treated 6061-TiC coating presented a mean SWR 25% lower than the AS-satellited 6061-TiC, despite the heat-treated coating yielding lower microhardness values. Therefore, the HT-satellited 6061-TiC coating presents a total reduction of ~70% and 40%

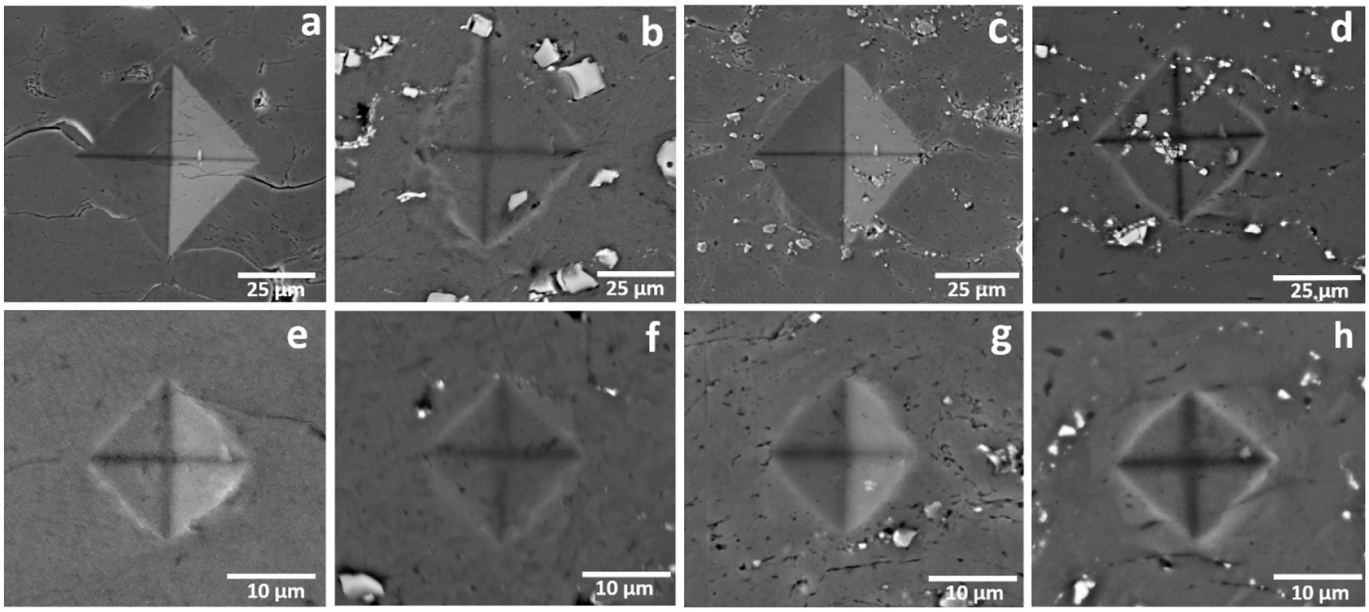

Fig. 9. SE images of microhardness indents of the deposited coatings at 50 gf (upper row) and 10 gf (lower row); (a and e) AS-6061, (b and f) AS-blended 6061-TiC, (c and g) AS-satellited 6061-TiC, (d and h) HT-satellited 6061-TiC.

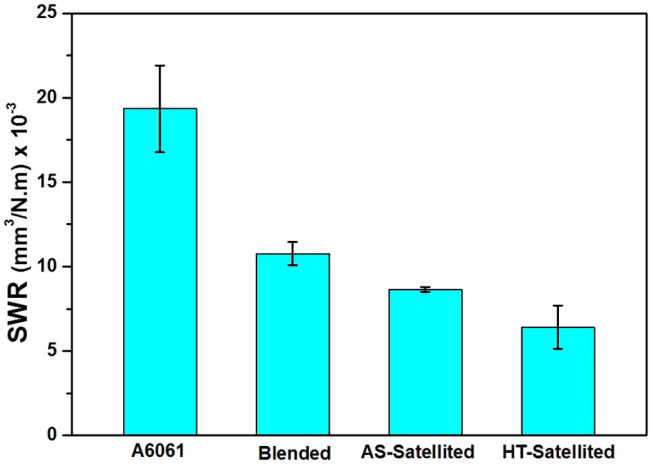

Fig. 10. The average SWR of the deposited coatings, showing the effect of the reinforcement and heat treatment on reducing the SWR.

in comparison to the 6061 and blended 6061-TiC coating, respectively. A likely explanation for this is the reduced porosity in the heat-treated coating due to annealing improving the resistance of the coating against wear. This is likely explained by a reduction in the incidence of a pull-out based wear mechanism which was observed in the wear tracks in this work. The pulling-out of the reinforcing particle has been reported as an important factor in increasing the wear rate in the composite coatings [49]. To further explain the wear behaviour of the deposited coatings, SE images at two magnifications are shown of the wear tracks in Fig. 11. 3D-view images of the entire wear track are also shown.

The as-sprayed 6061 coating exhibits a wear track morphology with a combination of abrasive scratches and flattened regions of the original splat morphology. Round regions can be seen with similar dimensions to individual deposits. These regions have no indication of grooving implying either a pull-out/delamination mechanism taking place, or these regions are particularly soft. In addition, wear debris has also become trapped between splat-like regions, likely explained by regions of porosity revealed during wear. It is clear therefore that in the case of the 6061 coating the inter-splat porosity and splat-based structure has an adverse influence on the wear mechanism. The blended 6061-TiC

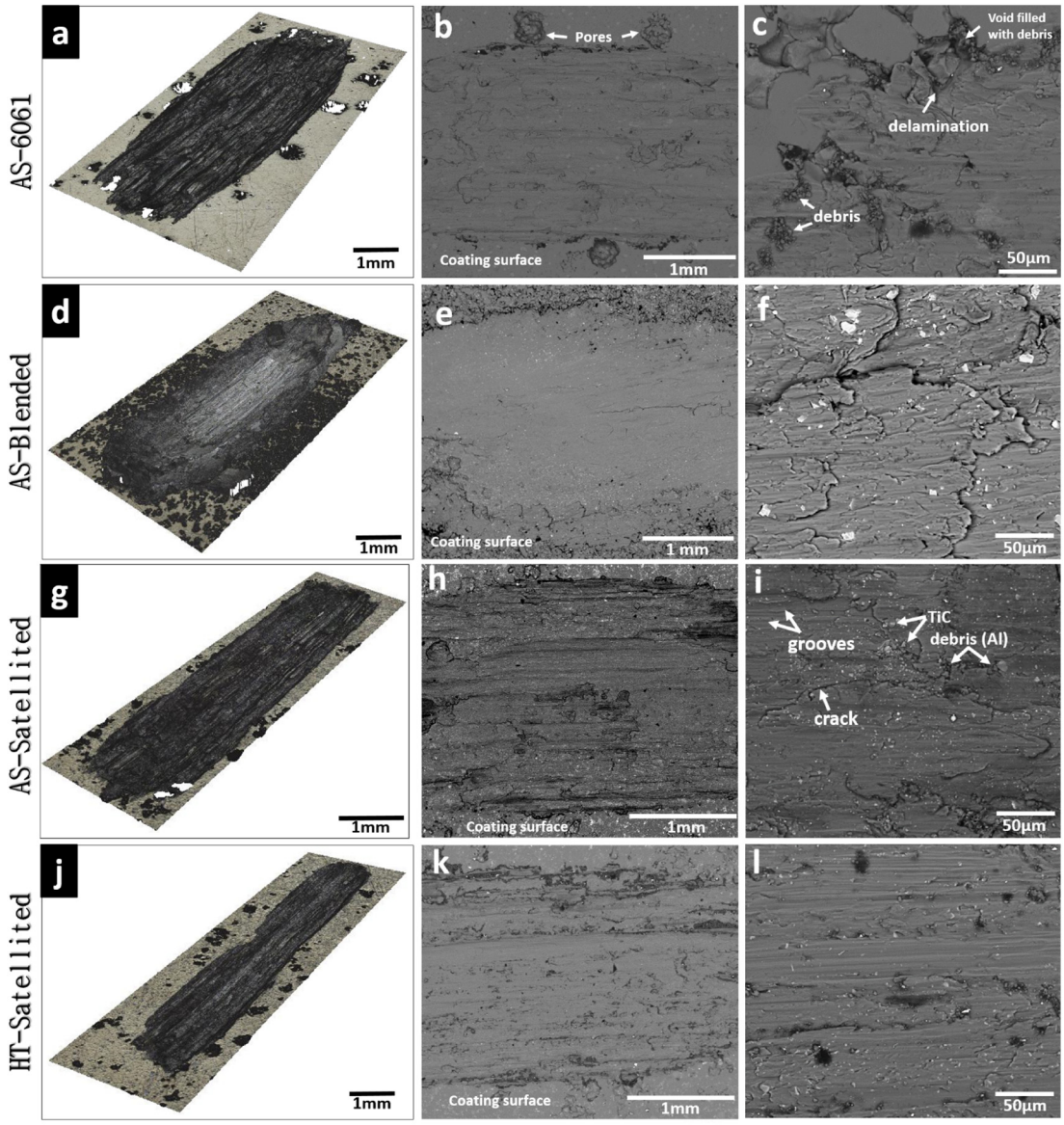

Fig. 11. Images of the worn surfaces; first column: 3D-views of the entire wear tracks; second column: low magnification SEM images; and third column: high magnification SEM images. Coating type was labelled at the lift-hand side.

coating shows excessive wear on the surface, with a combination of fracture and cracking confirmed by the high magnification image, Fig. 11-f. It is likely that the low reinforcement amount, weak cohesion and the high porosity in the blended coating overall produce a more severe wear process.

In the case of the satellited 6061-TiC coatings, splats do not appear as part of the wear morphology. Abrasive grooves dominate the surface, with cracking also prevalent. For the HT-satellited 6061-TiC coating, a similar abrasive mechanism can be seen with scratching apparently less prevalent. In the low magnification image, the wear morphology of the heat-treated coating appears somewhat more uniform than the untreated, providing evidence that more uniform properties pervade the coating. Several studies have considered toughness as a significant factor in the improved wear behaviour of metal matrix-ceramic composites [50,51]. Qiao et al. have also noted that there is a correlation with the bonding between the hard particles and the matrix, and the adhesion between splats and the toughness of the composite coating [52]. Improved bonding between ceramic particles and matrix in composite coatings can also lead to a reduction in the amount of pulled-out ceramic particles, which is a key mechanism in wear of such materials, and hence this improves the coating wear resistance [50]. Given the reduction of porosity, as a result of the heat treatment process in this work, these mechanisms based on improved cohesion may be contributing factors to the improved wear behaviour. Thus, the contribution of TiC particles in strengthening the coating has a clear impact on enhancing the wear resistance of the 6061-TiC coating. Furthermore, the HT-6061-TiC coating yielded the lowest SWR among the deposited coating, explained by enhanced cohesion owing to the heat treatment process.

4. Conclusions

In this work, the effect of using satelliting feedstock preparation on the deposition and characteristics of A6061-TiC coatings fabricated by cold-spray was investigated. The use of satelliting is shown to overcome typical defects observed in the deposition of less compliant Al alloys. Deposition efficiency of the 6061-TiC satellite feedstock was improved by 40% in comparison to that when using a simple 6061 feedstock, as the coating porosity reduced by ~70% with using the satellited feedstock. The TiC area fraction increased by > 60% in the satellited coating section compared to the blended coating. In addition, heat-treatment of the satellited coating at 345 °C for 2 h yielded a reduced porosity of 0.21% from 0.66% for the non-heat-treated coating. This was explained by reduced inter-particle interfaces and an enhanced coating-substrate interface owing to the solid state diffusion of Al. The contribution of the satelliting approach is manifested in increased embedment and enhancing the compaction action of TiC in the composite coating. The as-sprayed satellited 6061-TiC coating yielded the highest mean microhardness value among the coatings at 91 HV0.05 (± 1.5). The mean hardness of the heat-treated 6061-TiC was 83 HV0.05 (± 0.7), while the as sprayed 6061 coating yielded 70 HV0.05 (± 0.8). The blended 6061-TiC coating presented a hardness similar to the 6061 coating, 67 HV0.05 (± 1.8). Under dry-sliding conditions, the specific wear rate of the heat-treated 6061-TiC cold-sprayed coating against a steel ball was reduced by a mean of 25% in comparison to the as-sprayed coating, with good repeatability. This was explained by the contribution of the improved toughness and enhanced structure cohesion after heat treatment, resulting in reduced fracture during wear.

Acknowledgements

The authors would like to thank the Iraqi ministry of higher education for financial support of Mr. Al-Hamdani's studentship.

References

[1] L. Huang, L. Geng, Discontinuously Reinforced Titanium Matrix Composites: Microstructure Design and Property Optimization, Springer, 2017.
[2] R. Dasgupta, Aluminium alloy-based metal matrix composites: a potential material for wear resistant applications, ISRN metallurgy 2012 (2012).
[3] S. Gopalakrishnan, N. Murugan, Production and wear characterisation of AA 6061 matrix titanium carbide particulate reinforced composite by enhanced stir casting method, Compos. Part B 43 (2012) 302–308.
[4] B. Torres, M. Garrido, A. Rico, P. Rodrigo, M. Campo, J. Rams, Wear behaviour of thermal spray Al/SiCp coatings, Wear 268 (2010) 828–836.
[5] H.A. Murthy, S.K. Singh, Influence of TiC particulate reinforcement on the corrosion behaviour of Al 6061 metal matrix composites, Adv. Mater. Lett. 6 (2015) 633–640.
[6] K. Umanath, K. Palanikumar, S. Selvamani, Analysis of dry sliding wear behaviour of Al6061/SiC/Al2O3 hybrid metal matrix composites, Compos. Part B 53 (2013) 159–168.
[7] R. Shyu, C. Ho, In situ reacted titanium carbide-reinforced aluminum alloys composite, J. Mater. Process. Technol. 171 (2006) 411–416.
[8] M. Rokni, C. Widener, V. Champagne, Microstructural evolution of 6061 aluminum gas-atomized powder and high-pressure cold-sprayed deposition, J. Therm. Spray Technol. 23 (2014) 514–524.
[9] V. Champagne, D. Helfritch, Critical assessment 11: structural repairs by cold spray, Mater. Sci. Technol. 31 (2015) 627–634.
[10] S. Yin, Y. Xie, J. Cizek, E. Ekoi, T. Hussain, D. Dowling, et al., Advanced diamond-reinforced metal matrix composites via cold spray: properties and deposition mechanism, Compos. Part B 113 (2017) 44–54.
[11] K. Spencer, V. Luzin, N. Matthews, M.X. Zhang, Residual stresses in cold spray Al coatings: the effect of alloying and of process parameters, Surf. Coat. Technol. 206 (2012) 4249–4255.
[12] H. Assadi, H. Kreye, F. Gärtner, T. Klassen, Cold spraying–a materials perspective, Acta Mater. 116 (2016) 382–407.
[13] V.K. Champagne, The Cold Spray Materials Deposition Process: Fundamentals and Applications, Elsevier, 2007.
[14] A. Ganesan, J. Affi, M. Yamada, M. Fukumoto, Bonding behavior studies of cold sprayed copper coating on the PVC polymer substrate, Surf. Coat. Technol. 207 (2012) 262–269.
[15] O.C. Ozdemir, C.A. Widener, M.J. Carter, K.W. Johnson, Predicting the effects of powder feeding rates on particle impact conditions and cold spray deposited coatings, J. Therm. Spray Technol. 26 (2017) 1598–1615.
[16] A. Clare, A. Kennedy, Additive Manufacturing. Google Patents, (2014).
[17] V. De Simone, D. Caccavo, G. Lamberti, M. d'Amore, A.A. Barba, Wet-granulation process: phenomenological analysis and process parameters optimization, Powder Technol. 340 (2018) 411–419.
[18] K. Al-Hamdani, J. Murray, T. Hussain, A. Kennedy, A. Clare, Cold sprayed metal-ceramic coatings using satellited powders, Mater. Lett. 198 (2017) 184–187.
[19] H. Tan, D. Hao, K. Al-Hamdani, F. Zhang, Z. Xu, A.T. Clare, Direct metal deposition of TiB2/AlSi10Mg composites using satellited powders, Mater. Lett. 214 (2017) 123–126.
[20] F. Zhang, M. Mei, K. Al-Hamdani, H. Tan, A.T. Clare, Novel nucleation mechanisms through satelliting in direct metal deposition of Ti-15Mo, Mater. Lett. 213 (2017) 197–200.
[21] E. Irissou, J.-G. Legoux, B. Arsenault, C. Moreau, Investigation of Al-Al2O3 cold spray coating formation and properties, J. Therm. Spray Technol. 16 (2007) 661–668.
[22] W.Y. Li, C. Zhang, X. Guo, J. Xu, C.J. Li, H. Liao, et al., Ti and Ti-6Al-4V coatings by cold spraying and microstructure modification by heat treatment, Adv. Eng. Mater. 9 (2007) 418–423.
[23] M. Tajally, Z. Huda, H. Masjuki, A comparative analysis of tensile and impact-toughness behavior of cold-worked and annealed 7075 aluminum alloy, International journal of impact engineering 37 (2010) 425–432.
[24] N.M. Chavan, M. Ramakrishna, P.S. Phani, D.S. Rao, G. Sundararajan, The influence of process parameters and heat treatment on the properties of cold sprayed silver coatings, Surf. Coat. Technol. 205 (2011) 4798–4807.
[25] S.B. Pitchuka, D. Lahiri, G. Sundararajan, A. Agarwal, Scratch-induced deformation behavior of cold-sprayed aluminum amorphous/nanocrystalline coatings at multiple load scales, J. Therm. Spray Technol. 23 (2014) 502–513.
[26] R. Huang, M. Sone, W. Ma, H. Fukanuma, The effects of heat treatment on the mechanical properties of cold-sprayed coatings, Surf. Coat. Technol. 261 (2015) 278–288.
[27] A. Moridi, Powder Consolidation Using Cold Spray: Process Modeling and Emerging Applications, Springer, 2016.
[28] R. Fernandez, B. Jodoin, Cold spray aluminum–alumina cermet coatings: effect of alumina content, J. Therm. Spray Technol. 27 (2018) 603–623.
[29] K.I. Triantou, D.I. Pantelis, V. Guipont, M. Jeandin, Microstructure and tribological behavior of copper and composite copper+ alumina cold sprayed coatings for various alumina contents, Wear 336 (2015) 96–107.
[30] P. Chivavibul, M. Watanabe, S. Kuroda, K. Shinoda, Effects of carbide size and Co content on the microstructure and mechanical properties of HVOF-sprayed WC–Co coatings, Surf. Coat. Technol. 202 (2007) 509–521.
[31] T. Hussain, D. McCartney, P. Shipway, Impact phenomena in cold-spraying of titanium onto various ferrous alloys, Surf. Coat. Technol. 205 (2011) 5021–5027.
[32] Handbook A, Aluminum and Aluminum Alloys, ASM international, 1993, p. 117.
[33] S. Klinkov, V. Kosarev, Measurements of cold spray deposition efficiency, J. Therm. Spray Technol. 15 (2006) 364.
[34] A. Moridi, S.M. Hassani-Gangaraj, M. Guagliano, M. Dao, Cold spray coating:

review of material systems and future perspectives, Surf. Eng. 30 (2014) 369–395.
[35] K. Spencer, D. Fabijanic, M.-X. Zhang, The use of Al–Al2O3 cold spray coatings to improve the surface properties of magnesium alloys, Surf. Coat. Technol. 204 (2009) 336–344.
[36] Y.-K. Wei, X.-T. Luo, C.-X. Li, C.-J. Li, Optimization of in-situ shot-peening-assisted cold spraying parameters for full corrosion protection of Mg alloy by fully dense Al-based alloy coating, J. Therm. Spray Technol. 26 (2017) 173–183.
[37] H. Assadi, T. Schmidt, H. Richter, J.-O. Kliemann, K. Binder, F. Gärtner, et al., On parameter selection in cold spraying, J. Therm. Spray Technol. 20 (2011) 1161–1176.
[38] M. Rokni, S. Nutt, C. Widener, V. Champagne, R. Hrabe, Review of relationship between particle deformation, coating microstructure, and properties in high-pressure cold spray, J. Therm. Spray Technol. 26 (2017) 1308–1355.
[39] H. Koivuluoto, P. Vuoristo, Effect of ceramic particles on properties of cold-sprayed Ni-20Cr + Al2O3 coatings, J. Therm. Spray Technol. 18 (2009) 555.
[40] Y.T.R. Lee, H. Ashrafizadeh, G. Fisher, A. McDonald, Effect of type of reinforcing particles on the deposition efficiency and wear resistance of low-pressure cold-sprayed metal matrix composite coatings, Surf. Coat. Technol. 324 (2017) 190–200.
[41] C.A.M. Grard, Aluminium and Its Alloys, (1922).
[42] B. Messer, S. Dais, D. Wolf, Detection of vacancy-induced self-diffusion by rotating-frame spin-lattice relaxation in aluminum, Paper From “Magnetic Resonance and Related Phenomena”, 1975, p. 2.
[43] F. Van Loo, G. Rieck, Diffusion in the titanium-aluminium system—I. Interdiffusion between solid Al and Ti or Ti-Al alloys, Acta Metall. 21 (1973) 61–71.
[44] A. Okura, K. Motoki, Rate of formation of intermetallic compounds in aluminium matrix-carbon fibre composites, Compos. Sci. Technol. 24 (1985) 243–252.
[45] Z. Arabgol, H. Assadi, T. Schmidt, F. Gärtner, T. Klassen, Analysis of thermal history and residual stress in cold-sprayed coatings, J. Therm. Spray Technol. 23 (2014) 84–90.
[46] R.-Y. Chen, H.-Y. Chu, C.-C. Lai, C.-T. Wu, Effects of annealing temperature on the mechanical properties and sensitization of 5083-H116 aluminum alloy, Proceedings of the Institution of Mechanical Engineers, Part L: Journal of Materials: Design and Applications 229 (2015) 339–346.
[47] E.L. Cantera, B. Mellor, Fracture toughness and crack morphologies in eroded WC–Co–Cr thermally sprayed coatings, Mater. Lett. 37 (1998) 201–210.
[48] C. Lee, J. Han, J. Yoon, M. Shin, S. Kwun, A study on powder mixing for high fracture toughness and wear resistance of WC–Co–Cr coatings sprayed by HVOF, Surf. Coat. Technol. 204 (2010) 2223–2229.
[49] M. Hashempour, H. Razavizadeh, H. Rezaie, Investigation on wear mechanism of thermochemically fabricated W–Cu composites, Wear 269 (2010) 405–415.
[50] J. Guilemany, S. Dosta, J. Miguel, The enhancement of the properties of WC-Co HVOF coatings through the use of nanostructured and microstructured feedstock powders, Surf. Coat. Technol. 201 (2006) 1180–1190.
[51] N. Melendez, V. Narulkar, G. Fisher, A. McDonald, Effect of reinforcing particles on the wear rate of low-pressure cold-sprayed WC-based MMC coatings, Wear 306 (2013) 185–195.
[52] Y. Qiao, T.E. Fischer, A. Dent, The effects of fuel chemistry and feedstock powder structure on the mechanical and tribological properties of HVOF thermal-sprayed WC–Co coatings with very fine structures, Surf. Coat. Technol. 172 (2003) 24–41.
[53] J.R. Davis, Aluminum and Aluminum Alloys, ASM international, 1993.